Nonlinear Deformation of a Ferrofluid Droplet in a Uniform Magnetic Field

Gui-Ping Zhu,[a] Nam-Trung Nguyen, [a] * R. V. Ramanujan,[b] and Xiao-Yang Huang [a]

[a] School of Mechanical and Aerospace Engineering, Nanyang Technological University, 50 Nanyang Avenue, Singapore, Singapore 639798
[b] School of Material Science and Engineering, Nanyang Technological University, 50 Nanyang Avenue, Singapore, Singapore 639798

*To whom correspondence should be addressed. E-mail: mntnguyen@ntu.edu.sg.

Abstract

This paper reports experimental and numerical results of the deformation of a ferrofluid droplet on a super hydrophobic surface under the effect of a uniform magnetic field. A water-based ferrofluid droplet surrounded by immiscible mineral oil was stretched by a magnetic field parallel to the substrate surface. The results show that an increasing flux density increases the droplet width and decreases the droplet height. A numerical model was established to study the equilibrium shape of the ferrofluid droplet. The governing equations for physical fields, including the magnetic field, are solved by the finite volume method. The interface between the two immiscible liquids was tracked by the level-set method. Nonlinear magnetization was implemented in the model. Comparison between experimental and numerical results shows that the numerical model can predict well the nonlinear deformation of a ferrofluid droplet in a uniform magnetic field.

Introduction

The shape of a liquid droplet is of great interest for the field of droplet-based microfluidics. Under gravitational distortion, the shape of a sessile droplet has been numerically investigated with varying degrees of success. The classic numerical solutions from Bashforth and Adams was widely employed.[1] Robertson and Lehman obtained the shape by minimizing the total energy of the droplet with a constant mass.[2] By means of singular perturbation techniques, O'Brien et al. developed an asymptotic expression to estimate the shape of small sessile and pendant droplets.[3, 4] The study of droplet shape is particularly important as the solutions can be directly compared with experimental results.[5] In addition, the shape of the droplet allows an indirect measurement of surface tension.[6, 7]

Numerous techniques have been developed for controlling the behavior of a liquid droplet on a solid surface. Droplet behavior can be controlled by chemical gradient,[8] thermocapillarity,[9, 10] and electrostatic forces.[11, 12] Magnetic force was used in our previous work to control the behavior of a sessile ferrofluid droplet under the effect of a non-uniform external magnetic field.[13] This work indicated that the ferrofluid droplet undergoes a shape deformation. In the present paper, magnetic field was applied uniformly to investigate the deformed shape of a ferrofluid droplet.

Compared to the case of droplets flattened purely by gravitational force, the equilibrium shape of droplets in a magnetic field is difficult to obtain. Extra efforts are required to solve the problem involving non-local forces which depend on the shape of the domain occupied by the droplet. Sneyd and Moffatt presented a preliminary theory for predicting the equilibrium shape of a sessile ferrofluid droplet under a magnetic force.[14] The theory was derived based on potential energy minimization and perturbation method. The effects of both gravitational and magnetic force were examined on both wetting and non-wetting droplets. For droplet elongation under an external magnetic field, hysteresis phenomena were first experimentally investigated by Brancher and Zouaoui.[15] The phenomenon of hysteresis was further confirmed by the numerical results which presented the interface wavelength for the case of a wetting droplet. Bormashenko and Whyman proposed a universal solution to treat interactions

between a droplet and the surrounding as a generalized potential.[16] The application of standard calculus of variations was demonstrated to be effective and accurate for solving this problem.[17]

Previously, Rosensweig studied the deformation and instability of freely suspended droplets.[18] Numerical studies were carried out to obtain the deformation of both freely suspended droplets and sessile droplets in a uniform magnetic field.[19, 20] The resulting droplet shape is determined by the interaction between interfacial tension and magnetic force. Afkhami et al. presented experimental and numerical results exploring equilibrium state of a suspended hydrophobic ferrofluid droplet under a uniform magnetic field.[21, 22] Korlie et al. implemented a numerical model for a ferrofluid droplet falling down in a non-magnetic medium using a volume of fluid (VOF) method,[23] the ferrofluid in this model was taken to be linearly magnetized. The numerical study of nonlinearly magnetized ferrofluid droplet showed similar results with linear magnetized droplets at low magnetic field strengths.[24] Lavrova et al. also implemented the simulation of a nonlinearly magnetized ferrofluid droplet using finite element method (FEM).[20, 25]

Tracking the interface movement is a critical issue in the simulation of a multiphase system. There are different strategies proposed to describe the interface location. Level-set method (LSM) was demonstrated by Osher and Sethian for predicting the interface in a fixed-grid system.[26] Scardovelli and Zaleski reviewed the VOF method for predicting the moving interface.[27] To compare the accuracy of predicting the interface location, both methods were tested for flows with large vorticity.[28, 29] In the present work, level set method is used with reinitialization strategy to improve mass conservation.

In this paper, we describe the deformation of a sessile ferrofluid droplet on a hydrophobic surface under the effect of an applied magnetic field. The uniform magnetic field is generated by an electromagnet. The ferrofluid droplet is inserted into the air gap between the coils. The magnetic field is oriented parallel to the substrate surface. A sample container filled with mineral oil is required for the experiment. Mineral oil prevents liquid evaporation and makes the surface apparently superhydrophobic due to the thin film of oil between the substrate and the ferrofluid droplet. In the experiments, the geometry of the droplet was recorded while the

flux density of the applied magnetic field was varied with the applied current. A numerical model with non-linear magnetization was implemented to study the droplet shape under an applied uniform magnetic field coupled with interfacial tension and gravitational forces. The finite volume method is used to solve the governing equations. Interface tracking is achieved by level-set method.

Experimental Description

Materials and Methods

Figure 1 shows the schematic setup of the experiments reported in this paper. The planar surface used in the experiment was prepared on a Pyrex glass wafer. In order to obtain the hydrophobic properties, we treated the surface using the method reported by Long et al.[30] Readers may refer to our previous work for the detailed procedure of the preparation of the surface.[13] The sample container for was made of polymethylmethacrylate (PMMA). The size of the container was determined by the available slot between the two poles of the electromagnet. The PMMA holder was machined by laser cutting. The container was assembled by gluing pieces of PMMA together using chloroform. The pretreated planar surface was placed at the bottom of the container. The droplet was surrounded by mineral oil to improve the hydrophobic property of the contact and to prevent evaporation. Water based ferrofluid (EMG707, Ferrotec, USA) was used with 1.8-vol% 10-nm Fe_3O_4 nanoparticles. The viscosity of the ferrofluid at 27 ºC is 5 mPa s. The initial susceptibility is $\chi = 0.36$. The surface tension of the ferrofluid and air is 50 mN/m. The density is ρ=1.1 g/cm^3 at 25 ºC. The density of mineral oil (M5904 Sigma) at 25 ºC is ρ=0.84 g/cm^3.

We used a micropipette (Finnpipette, Thermo Scientific, USA) for dispensing the ferrofluid droplet. This micropipette is capable of accurately controlling liquid volumes ranging from 0.5 µL to 10 µL.

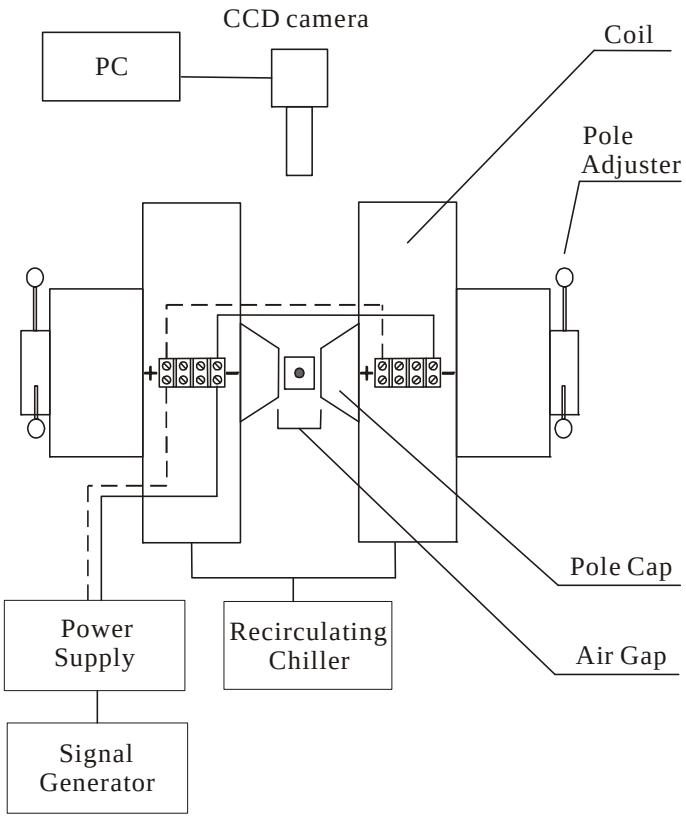

Figure 1: Experimental setup and imaging system (top view, not to scale, gravity direction is going into the view plane).

A continuous variable gap electromagnet (EM4 Series, Lake Shore, USA) generates the uniform magnetic field for the experiments. Adjusting the variable air gap between the poles can tune the range of the field strength. Once the gap is fixed, the field is controlled by the current input (0~70 A). Good alignment of the tapered pole caps ensures the stability and the uniformity of the magnetic field. Due to the large amount of heat generated in the coil, we used a recirculating chiller (NESLAB Merlin M100, Cole-Parmer, USA) for cooling. For a specific value of the field strength, one can refer to the chart given in the manufacturer's manual sheet and the calibration using a gaussmeter (Model 410, Lake Shore, USA). In our experiment, we fixed the air gap at 20.1 mm. For this air gap, a maximum flux density of approximately 1.55 T can be achieved with a current of 70 A. Figure 2 shows the measured data as the square dots, which agree well with the calibration curves provided by the manufacturer.

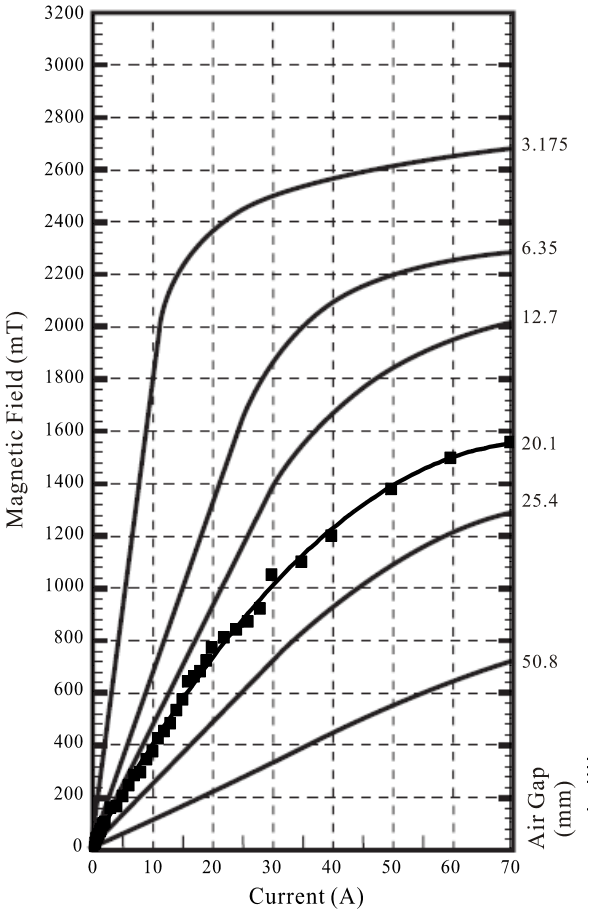

Figure 2: Magnetic flux density versus applied current calibration curves of the electromagnet used in the experiments. The data points are measured using a gaussmeter.

A CCD camera (Pulnix, progressive scan camera, JAI Inc., Japan) captured the images of the ferrofluid droplets for further processing. The camera was mounted horizontally to record the side view of the ferrofluid droplet. A scale was inserted and imaged as a reference for the calibration of the pixel values. A customized MATLAB program processed the images and evaluated the shape of the ferrofluid droplets. The image files were evaluated to extract parameters such as the width and the height of the droplet.

Results and Discussion

For ferrofluid droplets surrounded by a non-magnetizable medium, the magnetic field induces a mismatch of the normal stress balance at the interface of the two liquids. This stress mismatch forces the droplet to elongate along the field direction. Figure 3 illustrates the balance of the forces at the interface. For analyzing the problem, the ferrohydrodynamic

(FHD) Bernoulli equation is used to relate the pressures of a gravitational flattened droplet in a magnetic field. Considering a sessile ferrofluid droplet of a inviscid, isothermal and incompressible ferrofluid, the FHD Bernoulli equation is written as,[19]

$$p^* + \Delta\rho g z - p_m = Const \tag{1}$$

with the boundary condition,

$$p^* + p_n = p_0 + p_c \tag{2}$$

where n is the unit vector normal to the interface, $\Delta\rho$ is the density difference between the ferrofluid and the surrounding fluid; $p_m = \mu_0 \int_0^H M dH$ is the fluid-magnetic pressure with H and M the applied field strength and the corresponding magnetization parallel to the applied magnetic field; $p_n = \mu_0 M_n^2 / 2$ is the magnetic normal pressure with M_n representing the normal component of the magnetization; $p_c = 2C\sigma$ is the capillary pressure with σ and C indicating the surface tension and the radius of curvature; p_0 represents the pressure in the nonmagnetic fluid; and $p^* = p(\rho, T) + p_m$ is defined as the composite pressure with $p = p(\rho, T)$ representing the thermodynamic pressure in the magnetizable fluid before polarization. The permeability of vacuum has a value of $\mu_0 = 4\pi \times 10^{-7}\ N \cdot A^{-2}$.

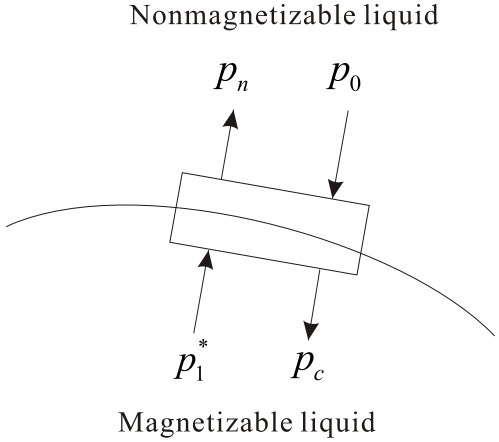

Figure 3: Force balance in a multiphase system with the magnetizable medium 1 and the nonmagnetizable medium 2.

At the interface, the magnetic surface force density can be expressed as[18]

$$t_{nn} = n \cdot T_m \cdot n = \mu_0 \int_0^H M dH + \frac{\mu_0}{2} M_n^2 \tag{3}$$

where T_m is the surface stress tensor for an incompressible nonlinear fluid. The surface force density directs from the magnetized to the non-magnetized phase. Eq. (3) indicates that the magnetic field strength and the corresponding magnetization of the ferrofluid determine the surface stress tensor, and consequently the elongation of the droplet.

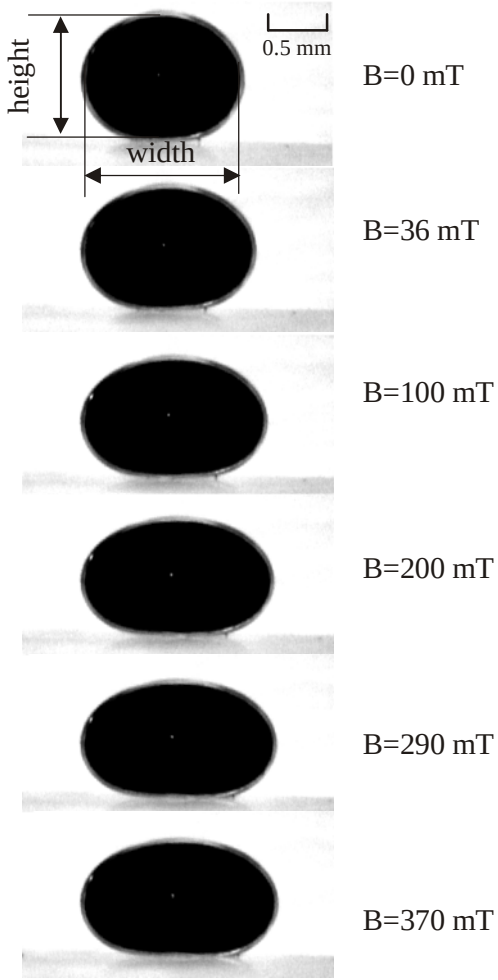

Figure 4: Deformation of a sessile ferrofluid droplet under different magnetic flux densities (V=1.3 μL).

We first investigated the effect of uniform magnetic flux density on the shape of a sessile ferrofluid droplet on a super hydrophobic surface. Figure 4 shows the typical shapes of a sessile ferrofluid droplet under different magnetic flux densities. The droplet is elongated along the direction of the field. Figure 5 shows the measured geometric parameters (height and width) of the different sessile ferrofluid droplets as a function of the flux densities. The size of the droplet does not affect the trend of the curve. The results show that a stronger magnetic field would stretch the ferrofluid droplet, increasing the width and decreasing the

height. It is worth noting that the width and height of the droplet remains constant upon reaching the saturated magnetization. The solid lines are fitting curves. Hysteresis phenomena were present in the behavior of the droplets. To investigate the hysteresis effect in the experiment, data was recorded for both magnetic loading and unloading processes. The arrows in Figure 5 indicate the loading process with increasing flux density and the unloading process with decreasing flux density. The intrinsic hysteresis in the system can be investigated by the discrepancy between the two curves.

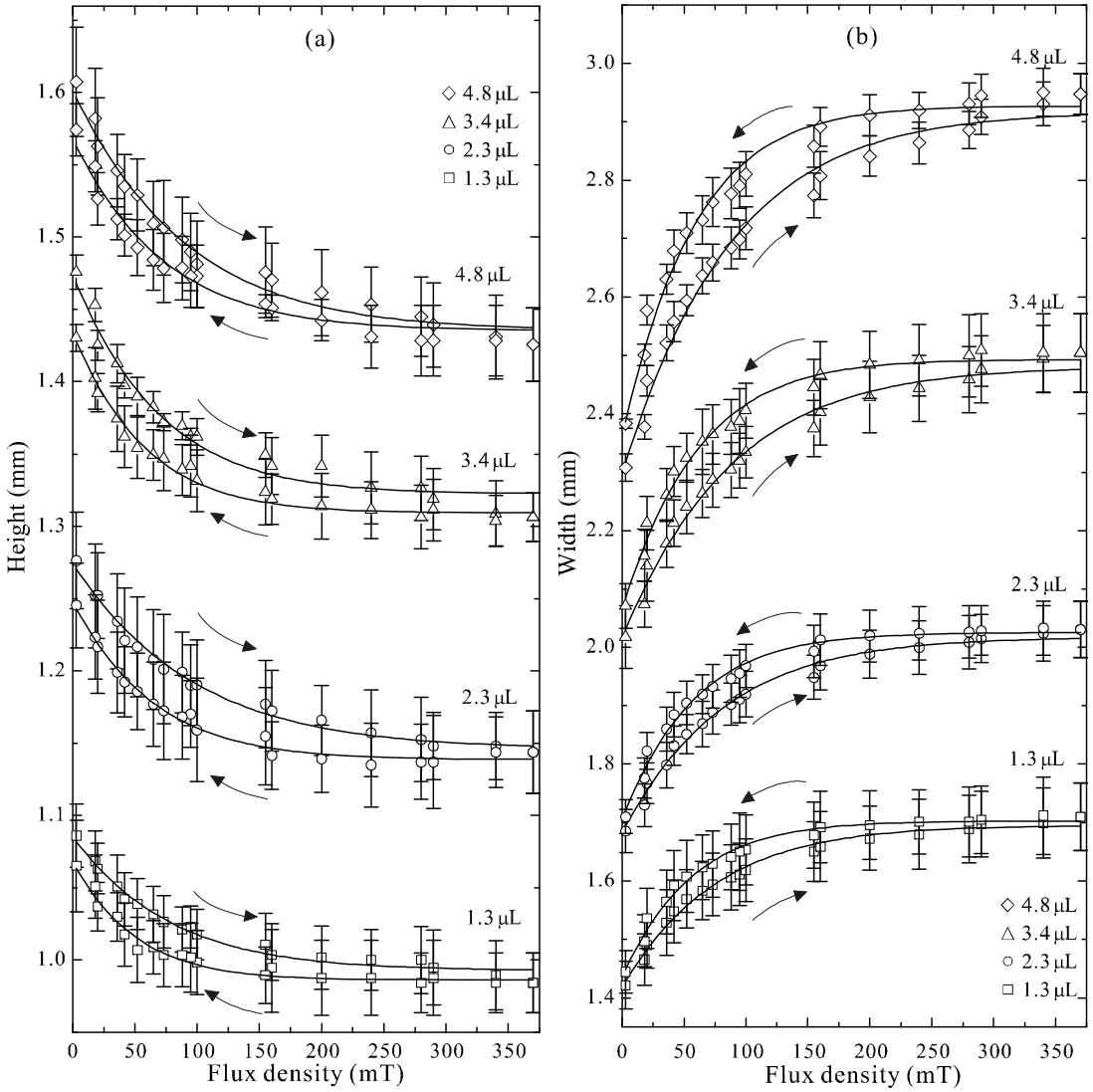

Figure 5: Experimental result of droplet parameters as a function of flux density: (a) height; (b) width.

The magnetic particles of a colloidal ferrofluid are dispersed in the paramagnetic fluid. However, these particles carry magnetic moments. In the absence of an external magnetic

field, dipole directions are random. The magnetic particles are polarized by orienting their dipole moments in the direction of the applied field. During the magnetization process, the angle between dipole moment and field direction becomes smaller as magnetic flux density increases. At a given value, the magnetic flux density is so high that the dipole moments may be completely aligned and saturation magnetization is achieved. The stretching behavior would be decreased or even stopped if the magnetic field increases further, as shown in the experimental curve. The magnetization M of a ferrofluid is a vector with the same direction as the applied field. The magnitude of magnetization follows the Langevin law as a function of the field strength H [31]

$$M(H) = M_s L(\gamma H) = M_s \left[\coth(\gamma H) - \frac{1}{\gamma H} \right] \tag{4}$$

where M_s is the saturation magnetization, and $\gamma = 3\chi_0 / M_s$ with χ_0 the initial value of magnetic susceptibility.

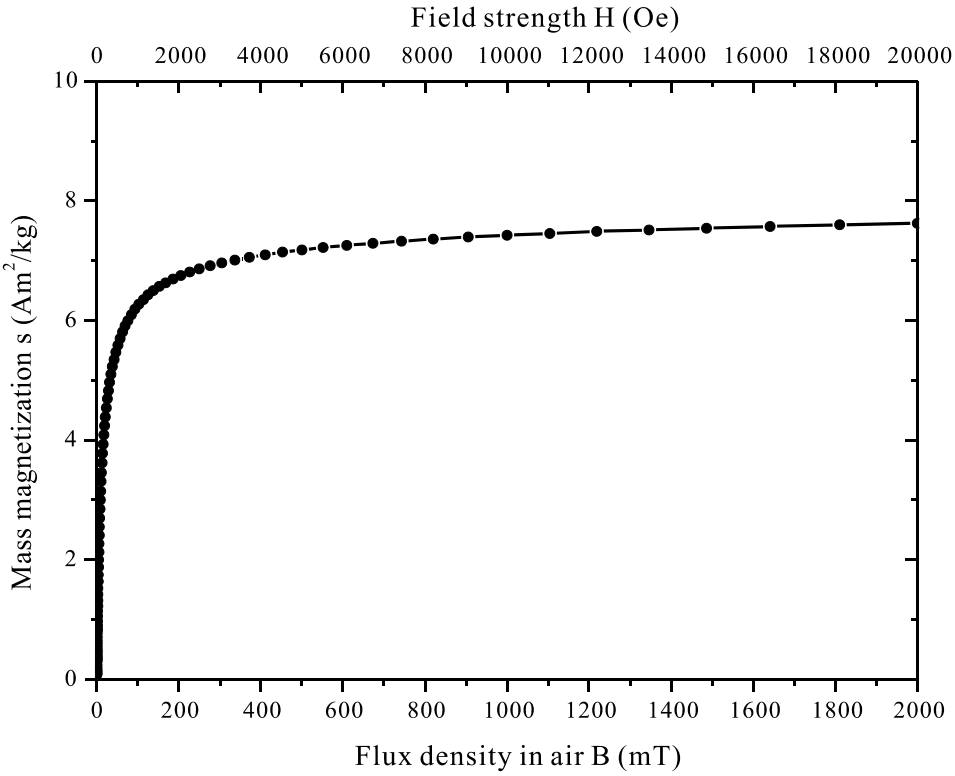

Figure 6: Magnetization curves of the ferrofluid used in our experiments (EMG707, Ferrotec, at 285K).

The magnetization data in Figure 6 was obtained from the manufacturer's data sheet. The magnetization M is calculated from the depicted mass magnetization s as $M = s\rho$, where

ρ is the density of the ferrofluid. Saturation magnetization of the ferrofluid is reached if the magnetic flux density in air is about 500 mT. Figure 7 shows the parameters of droplet as a function of magnetization. The specific mass magnetization values in Figure 7 were obtained through fourth-order Newton's interpolating polynomials.

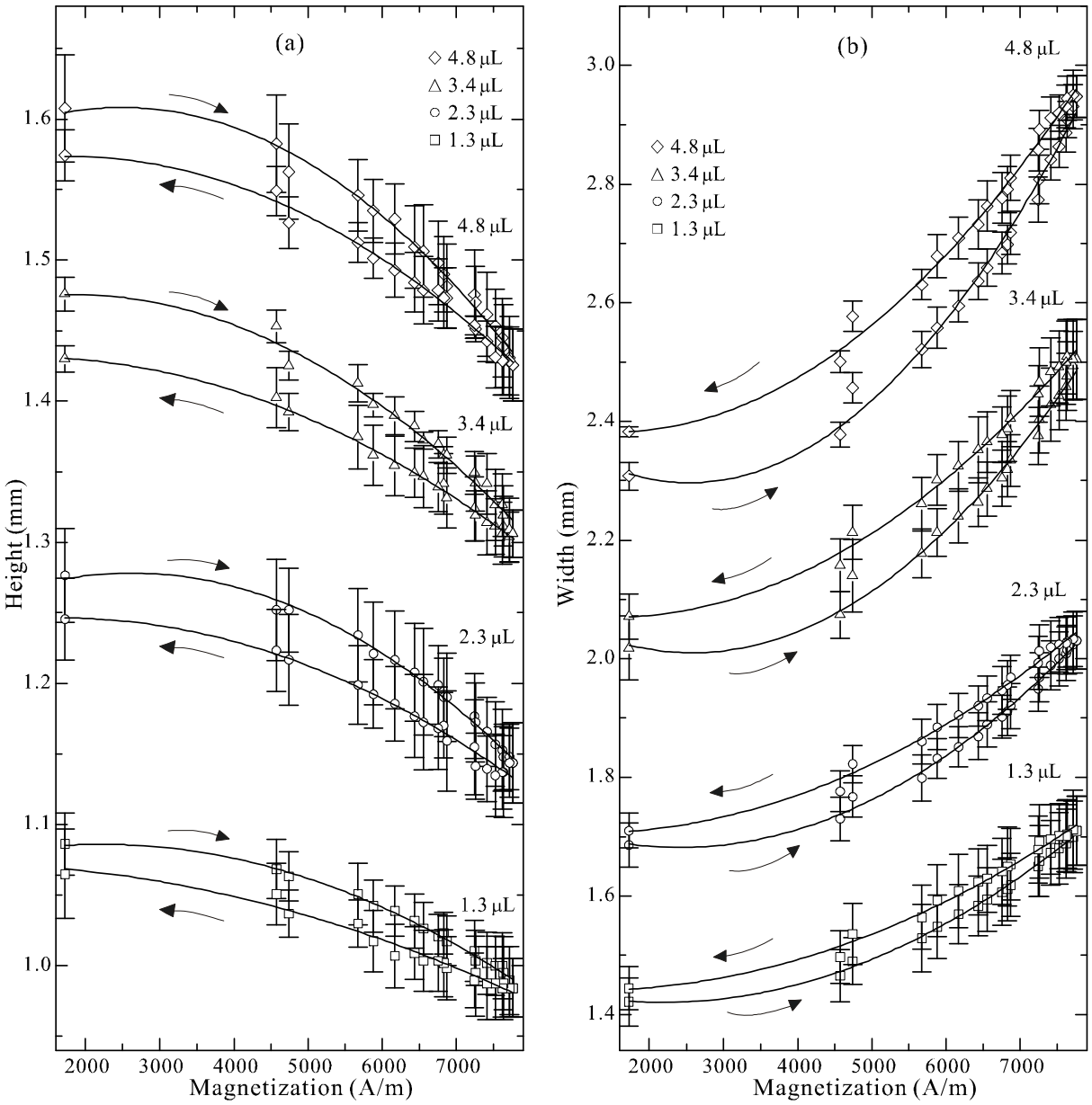

Figure 7: Experimental results of droplet parameters as a function of magnetization (with 2nd-order polynomial fit): (a) height; (b) width.

The Langevin's magnetization law as shown in Figure 6 can systematically describe the super paramagnetic properties in the ferrofluid. Because of the large magnetic flux density, the droplet in our experiment actually undergoes nonlinear magnetization. For a small flux

density, the deformation is significantly affected by the applied flux density. Figure 6 shows that the magnetization increases dramatically with an increasing flux density. In the range of flux density from 150 mT to 370 mT, the characteristic parameters of the droplets remain almost constant if depicted as function of the flux density. The relationship between the droplet parameters and the magnetization is better represented using the actual magnetization data of the ferrofluid droplet.

Numerical Simulation

Governing Equations

Except for the jump at the interface, the properties of a two-phase system are continuous. Thus, the governing equations of a continuum are still valid for describing the physical field inside each phase. Assuming a unsteady, incompressible, viscous, immiscible multi-phase system, the continuity and momentum equations are expressed as,

$$\frac{\partial \rho}{\partial t} + \nabla \bullet \left(\rho \vec{u} \right) = 0 \tag{5}$$

$$\frac{\partial}{\partial t}\left(\rho \vec{u} \right) + \nabla \bullet \left(\rho \vec{u} \vec{u} \right) = -\nabla P + \nabla \bullet \left[\mu \left(\nabla \vec{u} + \nabla \vec{u}^{T} \right) \right] + \vec{F} \tag{6}$$

where $\vec{u}$ is the velocity vector, and P is the pressure. For the case of a ferrofluid droplet under the effect of magnetic force, the force per unit volume $\vec{F}$ consists of gravitational force $\vec{F}_g$, interfacial tension force $\vec{F}_\sigma$ [32, 33] and magnetic force $\vec{F}_m$ [34]. Besides, the magnetic field also needs to be calculated. Magnetic potential is incorporated into the model according to:[34]

$$\nabla \bullet \left[\left(1 + \chi_m \right) \nabla \psi \right] = 0 \tag{7}$$

where χ_m is the ferrofluid susceptibility, and ψ is the magnetic scalar potential. The magnetic potential is introduced in the form of $\vec{H} = -\nabla \psi$ with $\vec{H}$ the magnetic field strength. For a magnetizable liquid, the Langevin's magnetization function in Eq.(4) is assumed and incorporated into the Maxwell equations. The susceptibility in Eq.(7) is taken to be

$$\chi_m = \frac{M_s}{H}\left[\coth(\gamma H) - \frac{1}{\gamma H}\right] \tag{8}$$

Due to discontinuity across the interface, properties within the whole computational domain are defined using the smoothed Heaviside function $H(\phi)$ through arithmetic mean,

$$\alpha(\phi) = H\alpha_+ + (1-H)\alpha_- \tag{9}$$

or a harmonic mean

$$\frac{1}{\alpha(\phi)} = \frac{H}{\alpha_+} + \frac{(1-H)}{\alpha_-} \tag{10}$$

The smoothed Heaviside function $H(\phi)$ is defined as,[33]

$$H(\phi) = \begin{cases} 0 & \phi < -\varepsilon, \\ (\phi+\varepsilon)/(2\varepsilon) + \sin(\pi\phi/\varepsilon)/(2\pi) & -\varepsilon \le \phi \le \varepsilon, \\ 1 & \varepsilon < \phi, \end{cases} \tag{11}$$

The typically good value of ε is 1.5 of the grid cell length. In our numerical model, the density is calculated by the arithmetic method. The viscosity and magnetic susceptibility act as coefficient of diffusion term and can be solved through the harmonic approach. The governing equations are solved on a Cartesian staggered grid by finite volume method.

We used the level-set method[26] to track the interface between the ferrofluid and the surrounding oil. The motion of the interface was obtained through introducing a signed normal distance function from the interface. During the numerical calculation, a reinitialization strategy was applied to reset and ensure the level-set function to be a signed distance function of the interface.[35] The level-set function was solved within a narrow band around the interface. This narrow-band approach as implemented by Peng et al. showed that the accuracy of the numerical results is not affected.[36] The processing time would be reduced by one order of magnitude due to the application of the narrow-band approach. The level-set and reinitialization equations are Hamiltonians in special form and thus can be solved by high-order weighted essentially non-oscillatory (WENO) schemes. The total variation diminishing (TVD) Runge-Kutta method was used for time discretization.[37, 38]

Validations and Results

A three-dimensional (3D) numerical model was developed using the geometry from the experiment for a ferrofluid droplet surrounded by mineral oil. The initial size of the simulated droplet was set to be 4.8 μL, which was the largest size investigated in the experiment, for this size, the effect of gravity is also captured in the simulation. The whole computational area was meshed uniformly. Due to symmetry, a one-half model was implemented. No-slip boundary condition was employed at the wall. Symmetric boundary conditions were applied at the symmetric surface. At first, a grid-independent study was carried out. Two different meshes with $42\times34\times26$ CVs at a time step of $\Delta t=1\times10^{-3}$ s and $62\times50\times38$ CVs at a time step of $\Delta t=5\times10^{-4}$ s were used. Figure 8 shows that the difference between the solutions is relatively small. Thus, the mesh $42\times34\times26$ CVs at a time step of $\Delta t=1\times10^{-3}$ s was sufficiently precise to capture the droplet behavior in the computational domain.

At first, we measured the interfacial tension between the ferrofluid and the surrounding mineral oil by matching the shapes of the droplet from experiment and simulation without the magnetic effect. Without a magnetic force, the deformation of the droplet was determined by the gravitational force and interfacial tension force only. The simulation couples the interactions between gravitational forces and interfacial forces in the model. Numerical calculations were implemented for a variety of interfacial tension forces with other system parameters fixed. A constant value of interfacial tension between the ferrofluid and the surrounding medium was assumed. The value of the interfacial tension was determined when the numerically obtained droplet shape matches the experimental shape. Using this fitting method, the interfacial tension between the ferrofluid and the mineral oil was determined as 3.0×10^{-3} N/m.

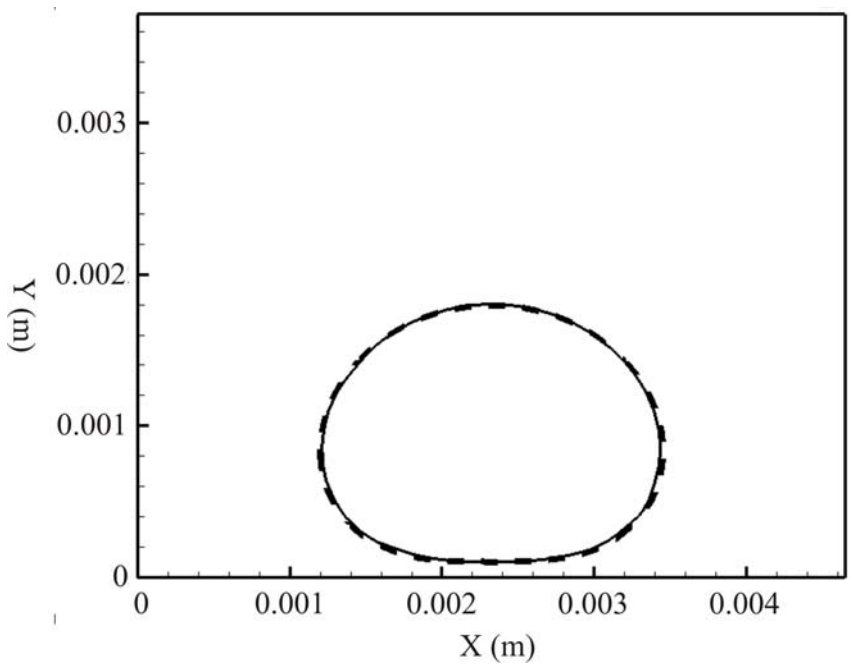

Figure 8: Grid-independent study with droplet in the computational domain (solid line: $42\times34\times26$ CVs at a time step of $\Delta t = 1\times10^{-3} s$, dashed line: $62\times50\times38$ CVs at a time step of $\Delta t = 5\times10^{-4} s$).

Figure 9 shows the comparison between experimental and simulation results of the droplet shape in the absence of a magnetic field. A thin oil film prevents the droplet from wetting the bottom surface. The numerical result is shown in Figure 9(b) where the solid black line represents the interfacial curve. The developed numerical model can accurately predict the deformation of the droplet considering the effects of gravity and interfacial forces only.

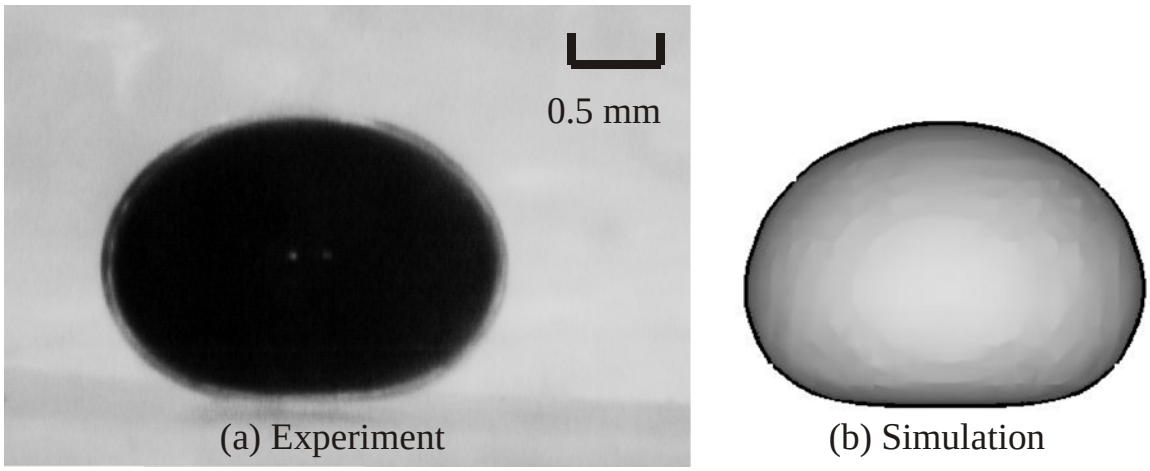

Figure 9: Comparison between experimental and numerical results (gravity flattened effect without magnetic force): (a) experiment; (b) simulation.

The magnetic force was then induced to study the effect on droplet deformation. The susceptibility mismatch between the two fluids enables the generation of magnetic force and thus the droplet deformation. In the experiments, the deformation of ferrofluid droplets occurred under a relatively high field strength. The magnetization curve in Fig. 6 shows that the region for droplets deformation is highly nonlinear. As ferrofluid droplets underwent nonlinear magnetization, the Langevin's magnetization law described by Eq.(4) was assumed and incorporated into the governing equation of the numerical model. Through numerical solution of Eq.(7), the magnetic potential was obtained, Figure 10. The arrow indicates the direction of the magnetic field H_0 which was introduced in the numerical calculations. For a ferrofluid droplet surrounded by a non-magnetizable medium, the sketch is shown for the initial shape and the final stretched shape.

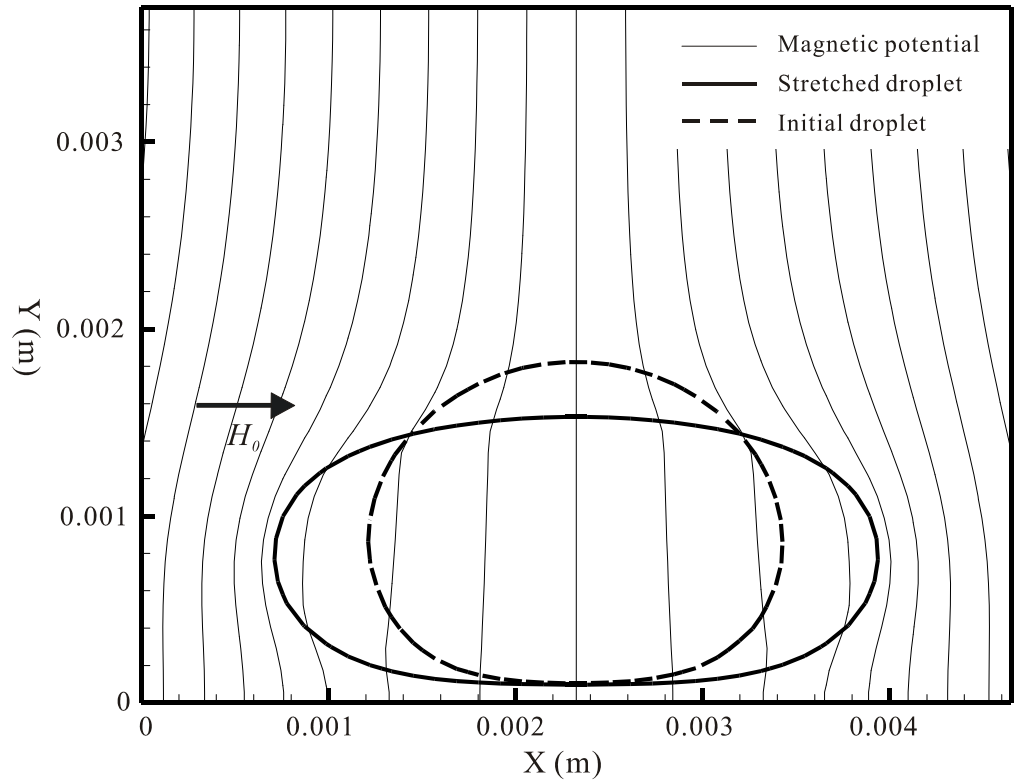

Figure 10: The magnetic potential for a sessile ferrofluid droplet in a uniform magnetic field.

The deformation of the droplets depends on both the magnetic susceptibility and the magnetic field strength. To generalize the investigation, the calculation was implemented with the magnetic Bond numbers B_m, which can be calculated from the properties of droplets and the applied magnetic field. The magnetic Bond number is defined as the ratio of

magnetic force to interfacial tension force

$$B_m = \frac{\mu_0 \chi V^{1/3} H_0^2}{2\sigma} \tag{12}$$

where H_0 is the applied magnetic field intensity and χ is the ferrofluid susceptibility. The volume of the droplet V is controllable in both experimental and numerical studies. The magnitude of the magnetic Bond number varies as the magnetic field strength changes. Figure 11 compares the experimental results with the numerical results of a 4.8-μL ferrofluid droplet. The deformation of a 4.8-μL droplet as observed in the experiments is shown in Figure 11(a).

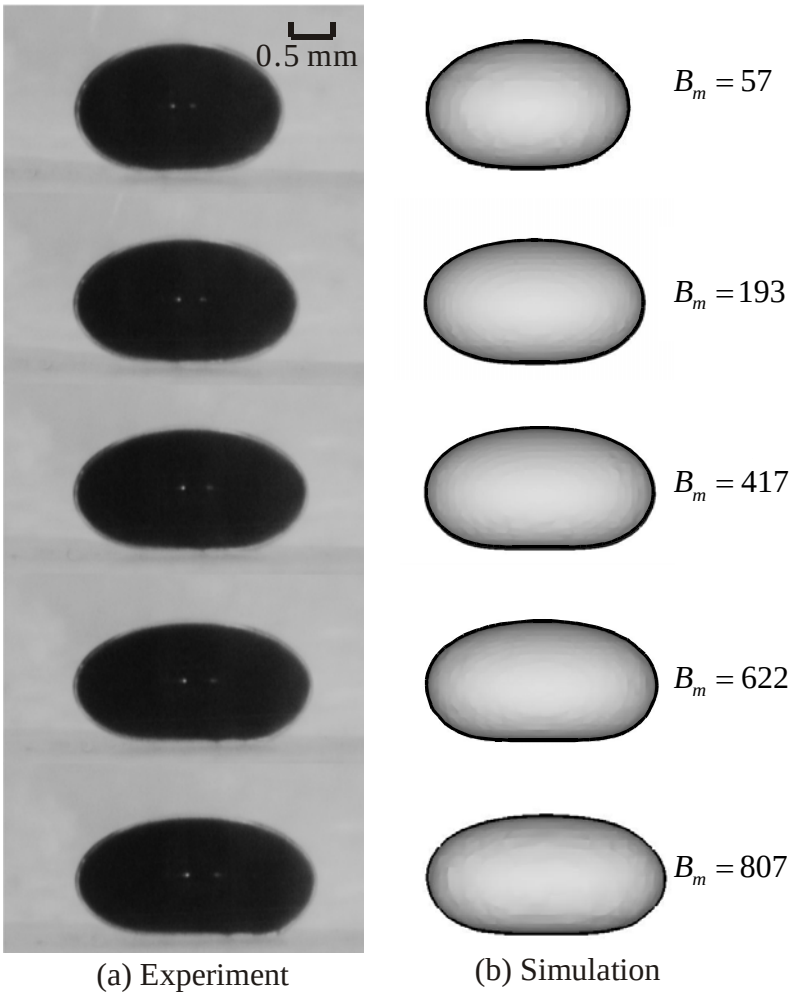

(a) Experiment (b) Simulation

Figure 11: The deformation of a ferrofluid droplet under different magnetic Bond numbers (V=4.8 μL): (a) experiment; (b) simulation.

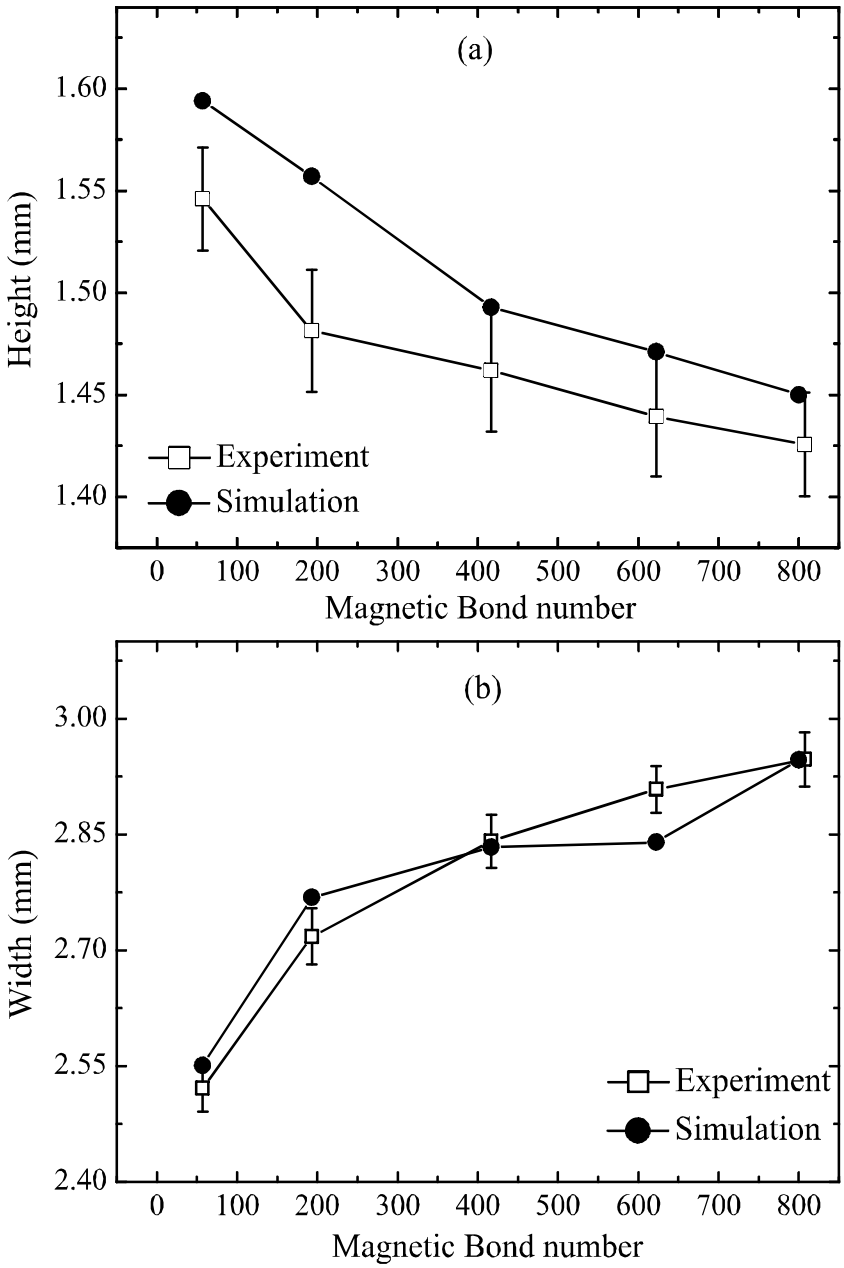

Figure 12: Geometrical parameters as functions of magnetic Bond number of a 4.8-μL ferrofluid droplet: (a) height; (b) width.

The numerical calculation was implemented with the value of magnetic Bond number corresponding to those used in the experiments, Figure 11(b). For different magnetic Bond numbers, the shapes of the droplet from the experiments agree well with the interfacial curve obtained from the simulation. The change of the width and the height of the droplet are compared in Figure 12. The higher magnetic Bond number leads to a further stretching of the droplet. The experimental results indicated that the stretching behavior decreases as magnetic Bond number increases. This nonlinear behavior agrees well with the trend predicted by the

numerical calculation. Although the experimental and numerical results show the same trend, the values differ slightly. The droplet height of simulation is slightly higher than that of the experiments. The discrepancy may be caused by the simplified numerical model.

Conclusions

This paper presents the deformation of a sessile ferrofluid droplet on a super hydrophobic surface under the influence of an external uniform magnetic field. The effect of an applied magnetic field on the droplet geometry was investigated through both experiment and numerical simulation. The droplet geometry for different magnetic flux densities was investigated experimentally. For nonlinear magnetized ferrofluid droplets, the Langevin's magnetization law was used in the numerical model. The nonlinear characteristics of the deformation of the droplet were captured well in the numerical model. Both experiment and simulation confirm the nonlinear relationship between geometric parameters of the droplet and the magnetic Bond number. The good agreement verifies that the numerical model can be used for the study of magnetic droplets in general and ferrofluid droplets in particular. The results indicate that using an external uniform magnetic field is an effective method for studying behavior of magnetic droplets. Furthermore, the results can be used for studying the phenomenon of magnetowetting or magnetic control of wettability for lab-on-a-chip applications.[39]

References

(1) Bashforth, F.; Adams, J. C. University Press: Cambridge, U.K., 1883.

(2) Robertson, W.; Lehman, G. *J. Appl. Phys.* **1968,** 39, (4), 1994-1996.

(3) O'Brien, S. B. G. *J. Fluid Mech.* **1991,** 233, 519-537.

(4) O'Brien, S. B. G. M.; Van Den Brule, B. H. A. A. *J. Chem. Soc., Faraday Trans.* **1991,** 87, (10), 1579-1583.

(5) Extrand, C. W.; Moon, S. I. *Langmuir* **2010,** 26, (22), 17090-17099.

(6) Padday, J. F.; Pitt, A. R. *Proceedings of the Royal Society of London*, London, 1972.

(7) Shanahan, M. E. R. *J. Chem. Soc., Faraday Trans. 1* **1982,** 78, (9), 2701-2710.

(8) Aksay, I. A.; Hoge, C. E.; Pask, J. A. *J. Phys. Chem.-U.S.* **1974,** 78, (12), 1178-1183.

(9) David, S.; Sefiane, K.; Tadrist, L. *Colloids Surf., A* **2007,** 298, (1-2), 108-114.

(10) Nguyen, N. T.; Ting, T. H.; Yap, Y. F.; Wong, T. N.; Chai, J. C. K.; Ong, W. L.; Zhou, J.; Tan, S. H.; Yobas, L. *Appl. Phys. Lett.* **2007,** 91, (8), 084102-084102-3.

(11) Hayes, R. A.; Feenstra, B. *Nature* **2003,** 425, (6956), 383-385.

(12) Yi, U. C.; Kim, C. J. *J. Micromech. Microeng.* **2006,** 16, 2053.

(13) Nguyen, N. T.; Zhu, G.; Chua, Y. C.; Phan, V. N.; Tan, S. H. *Langmuir* **2010,** 26, (15), 12553-12559.

(14) Sneyd, A. D.; Moffatt, H. K. *J. Fluid Mech.* **1982,** 117, 45-70.

(15) Brancher, J. P.; Zouaoui, D. *J. Magn. Magn. Mater.* **1987,** 65, (2-3), 311-314.

(16) Bormashenko, E.; Whyman, G. *Chem. Phys. Lett.* **2008,** 463, (1-3), 103-105.

(17) Arfken, G. B.; Weber, H. J. Harcourt Academic Press: 2001.

(18) Rosensweig, R. E. Cambridge University Press: New York, 1985.

(19) Sero-Guillaume, O. E.; Zouaoui, D.; Bernardin, D.; Brancher, J. P. *J. Fluid Mech.* **1992,** 241, 215-232.

(20) Lavrova, O.; Matthies, G.; Mitkova, T.; Polevikov, V.; Tobiska, L. *J. Phys.: Condens. Mat.* **2006,** 18, S2657.

(21) Afkhami, S.; Renardy, Y.; Renardy, M.; Riffle, J.; St Pierre, T. *J. Fluid Mech.* **2008,** 610, (-1), 363-380.

(22) Afkhami, S.; Tyler, A.; Renardy, Y.; RIFFLE, J. *J. Fluid Mech.* **2010,** 663, 358-384.

(23) Korlie, M. S.; Mukherjee, A.; Nita, B. G.; Stevens, J. G.; Trubatch, A. D.; Yecko, P. *J. Phys.: Condens. Mat.* **2008,** 20, 204143.

(24) Basaran, O. A.; Wohlhuter, F. K. *J. Fluid Mech.* **1992,** 244, 1-16.

(25) Lavrova, O.; Matthies, G.; Polevikov, V.; Tobiska, L. *PAMM* **2004,** 4, (1), 704-705.

(26) Osher, S.; Sethian, J. A. *J. Comput. Phys.* **1988,** 79, (1), 12-49.

(27) Scardovelli, R.; Zaleski, S. *Annu. Rev. Fluid Mech.* **1999,** 31, (1), 567-603.

(28) Rider, W. J.; Kothe, D. B. *12th AIAA CFD Conference*, San Diego, CA: United States, 1995.

(29) Rider, W. J.; Kothe, D. B. *J. Comput. Phys.* **1998,** 141, (2), 112-152.

(30) Long, Z.; Shetty, A. M.; Solomon, M. J.; Larson, R. G. *Lab Chip* **2009,** 9, (11), 1567-1575.

(31) Lavrova, O. Otto-von-Guericke-Universität Magdeburg, 2006.

(32) Brackbill, J.; Kothe, D. B.; Zemach, C. *J. Comput. Phys.* **1992,** 100, (2), 335-354.

(33) Yap, Y.; Chai, J.; Wong, T.; Toh, K.; Zhang, H. *Numer. Heat Tr. B-Fund.* **2006,** 50, (5), 455-472.

(34) Liu, J.; Tan, S. H.; Yap, Y. F.; Ng, M. Y.; Nguyen, N. T. *Microfluid. Nanofluid.* **2011,** 11, (2), 177-187.

(35) Sussman, M.; Smereka, P.; Osher, S. *J. Comput. Phys.* **1994,** 114, (1), 146–159.

(36) Peng, D.; Merriman, B.; Osher, S.; Zhao, H.; Kang, M. *J. Comput. Phys.* **1999,** 155, (2), 410-438.

(37) Jiang, G. S.; Shu, C. W. *J. Comput. Phys.* **1996,** 126, 202–228.

(38) Gottlieb, S.; Shu, C. W. *Math. Comput.* **1998,** 67, (221), 73-85.

(39) Tan, H.; Loke, W.; Tan, Y.; Nguyen, N. T. *Lab Chip* **2008,** 8, (6), 885.

TOC image